# Validated reduced computational methods for realistic RDC injection modeling

William Stumbar<sup>1a</sup>, William Stigliano<sup>2a</sup>, Jack Grunenwald<sup>3a</sup>, Peter Salek<sup>4b</sup>, Venkat Athmanathan<sup>5b</sup>, Terrence Meyer<sup>6b</sup>, Austin Webb<sup>7c</sup>, Chris Fugger<sup>8c</sup>, Kenji Miki<sup>9d</sup>, Doug Perkins<sup>10d</sup>, and James Braun<sup>11a</sup>

\*\*North Carolina State University, Raleigh, North Carolina\*\*

<sup>b</sup>Purdue University, West Lafayette, Indiana

<sup>c</sup>Spectral Energies LLC, Beaver Creek, Ohio

<sup>d</sup>NASA Glenn Research Center, Cleveland, Ohio

This paper outlines a simplified computational method without chemistry for single and multi-injector performance for rotating detonation combustion (RDC) environment as well as relevant performance metrics. For non-reactive cases, an unsteady pressure profile from a Method of Characteristics (MOC) simulation was used to simulate an RDC combustion wave travelling around the annulus. In reactive cases, a pre-mixed stoichiometric mixture of hydrogen and air is injected into a 2D unwrapped combustion chamber with an injector area. The performance is evaluated based on several performance metrics including unsteady discharge coefficient, average mass flux coming into the combustor, and percentage time obstructed. Finally, the computational method was validated through an experimental RDC test setup with a single element injector and hydrogen-air detonation drive.

#### Nomenclature

A = cross-sectional area of throat

C<sub>D</sub> = discharge coefficient f<sub>r</sub> = reduced frequency

 $f_w$  = frequency of detonation wave L = length of injector in meters

 $\dot{m}_{actual}$  = actual mass flow rate out of injector  $\dot{m}_{ideal}$  = ideal mass flow rate out of injector

MOC = method of characteristics

 $P_0$  = total pressure

 $P_{chamber}$  = average chamber static pressure

 $P_{feed}$  = feed total pressure

<sup>&</sup>lt;sup>1</sup> Graduate student, Department of Mechanical and Aerospace Engineering, wistumba@ncsu.edu

<sup>2</sup> Graduate student, Department of Mechanical and Aerospace Engineering

<sup>3</sup> Graduate student, Department of Mechanical and Aerospace Engineering

<sup>4</sup> Graduate student, Department of Mechanical and Aerospace Engineering

<sup>5</sup> Research Engineer

<sup>6</sup> Professor, Department of Mechanical Engineering

<sup>7</sup> Research Engineer

<sup>8</sup> Research Engineer

<sup>9</sup> Research Engineer

<sup>10</sup> Research Engineer

<sup>11</sup> Assistant Professor, Department of Mechanical and Aerospace Engineering

R = ideal gas constant

RDC = rotating detonation combustor RDE = rotating detonation engine

 $T_0$  = total temperature

 $U_{inj}$  = velocity of wave travelling back through the injector

γ = ratio of specific heats

 $\rho$  = density

#### I. Introduction

Rotating detonation combustors (RDCs) have known a significant area of research over the past couple of decades. RDCs utilize a detonation wave that travels around an annulus at a high frequency to combust the fuel/oxidizer. The fuel and oxidizer enter the combustor where it meets the high temperature, high pressure detonation wave that travels around the circumference of the annulus. The interaction causes the fuel and oxidizer to react and combust which results in a substantial pressure and temperature increase in the combustor. After the reaction, the products then exit, mostly axially, out of the open end of the combustor [1]. These combustors offer a list of potential advantages including their potentially high specific impulse, shorter engines, and possible pressure gain combustion [2]. Injection is a key area of interest due to the high mixing losses that occur, resulting in net pressure loss. Several researchers have investigated the optimization and the design of RDE injectors using steady numerical or experimental approaches [3-4].

Experimental efforts have been made toward determining how injectors perform based on their geometry and alignment [5-6]. The mixing of the fuel and oxidizer because of the injection is especially important as this can affect the performance and quality of the combustion with the RDC itself. Experimentation regarding variable mixing configurations has also been performed [6]. Experimental efforts have been made into studying the effects of a shock propagating through a square tube in relation to use in an RDC. Recovery time and mass deficit were calculated to determine the degree the injector is blocked and how long it takes the injector to inject again. Some other metrics were used to determine performance. It was found that a bilinear trend was present for recovery time in the cases that were tested [7].

Computational analysis of the mixing of RDC injectors has been performed along with a few unsteady injection studies with continuous detonation [8-9]. The unsteady nature of these combustors and the chemistry that must be simulated requires a high level of detail in the mesh and ultimately the solution that is produced. This high level of detail desires computationally expensive simulations requiring high levels of processing power and computational time. As a result, iterating these unsteady simulations over several different geometries and injector alignments can prove to be resource intensive. This necessitates a reduced model that can provide results over several different configurations while requiring less resources.

Current efforts lie in resolving the injector-combustor through detailed reactive 3D CFD calculations [19]. However, only a few publications deal with developing reduced order methods to model the effect of the detonation wave on the injector. Such methods are required to rapidly iterate over designs, but these methods also need to respect the fundamental two-dimensional flow features of the RDC to ensure similar refill times and characteristics are obtained. In the first part of the paper, a two-dimensional no-chemistry method to computationally assess the behavior of an RDC injector through boundary-layer resolved simulations is discussed through time-varying boundary conditions, extracted from an RDC model with chemistry. The goal is to utilize reduced computational methods to accurately simulate and predict injector performance for RDC applications. These results are then compared to a full 2D CFD simulation with the necessary combustion chemistry present and experimental results utilizing a single injector element in a constant detonation driver.

# II. 2D Approach

## A. 2D Method without chemistry

To simulate the environment the injector would be experiencing during an RDC experiment, a 2D domain was utilized. The two-dimensional geometry consists of an inlet plenum, outlet plenum, and a baseline injector. Some meshes of this domain are shown in Figure 1 below.

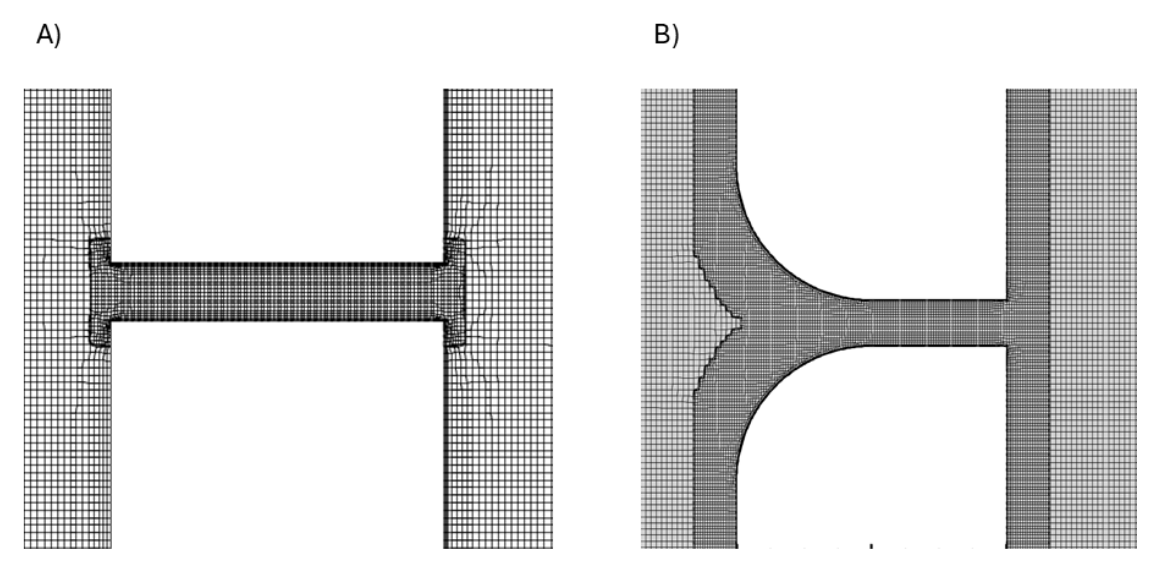


Figure 1: Straight Baseline Injector Geometries: A) Straight Baseline and B) Converging Baseline

Meshes of the geometries were created with FineOpen Hexpress and all the simulations were performed using Metacomp ICFD++ [10]. In CFD++, the simulation was set for a compressible, perfect gas that is assumed to be mostly above Mach 0.5. The simulation is of a transient nature using the 2-equation k-epsilon turbulence model built into CFD++. The boundary conditions imposed during the simulation are outlined in Figure 2. On the left side of Figure 2 are the boundary conditions used for the counterclockwise wave simulations while the one on the right outlines the clockwise wave simulations.

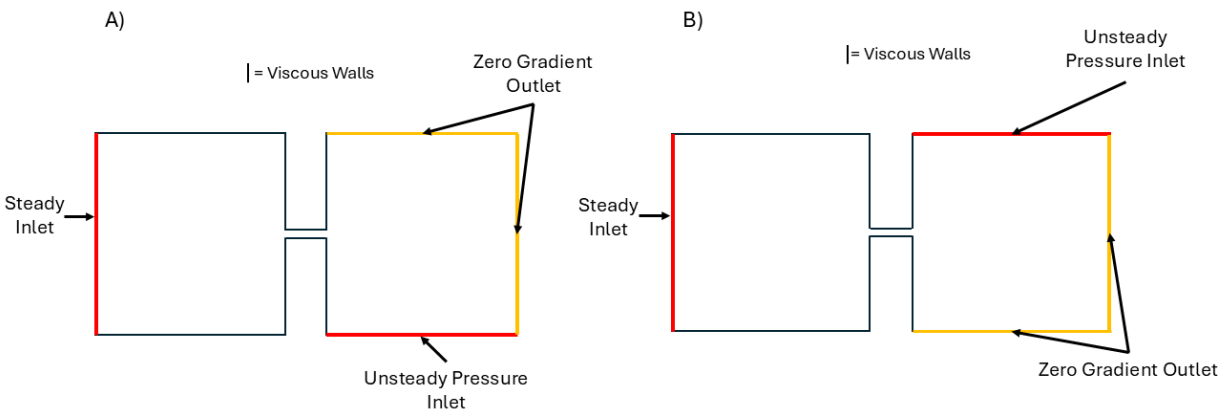


Figure 2: 2D Baseline Boundary Conditions: A) Counterclockwise wave and B) Clockwise wave

The leftmost boundary is a steady pressure inlet that can be adjusted to find the effects of feed total pressure on the performance of the injector. The rightmost boundary along with the top right boundaries are zero gradient outlets. This simulates the situation as if were a section of the RDC with the wave continuing to travel around the annulus (travelling through the top boundary) and travelling out of the RDC (right boundary). All the black boundaries are viscous walls. The unsteady pressure inlet is where a pressure pulse is imposed to simulate the detonation wave. Several different pulse profiles were utilized for testing this domain. The profile was created from an inlet slice of an inhouse RDE model based on the method of characteristics [11]. This profile is shown in Figure 3. The time step that was used for these pulse profiles is 0.48 µs with 150 maximum internal iterations.

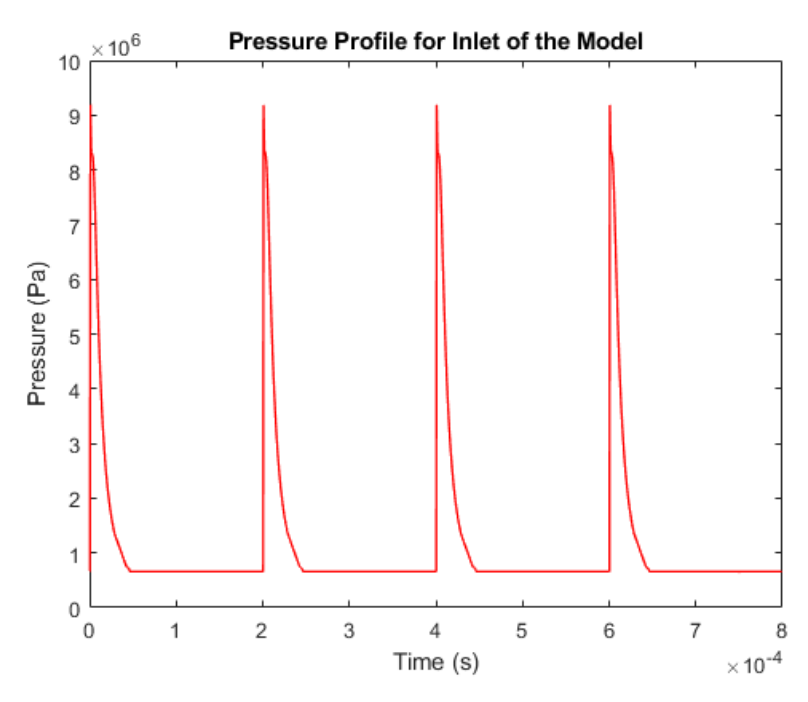


Figure 3: Inlet Pressure Profile for Imposed RDC Wave

The location of the axial slice that was taken to create this profile is shown in the Mach number contour from the MOC model of an "unwrapped" RDC annulus in Figure 4, which is detailed in Grunenwald et al. [11].

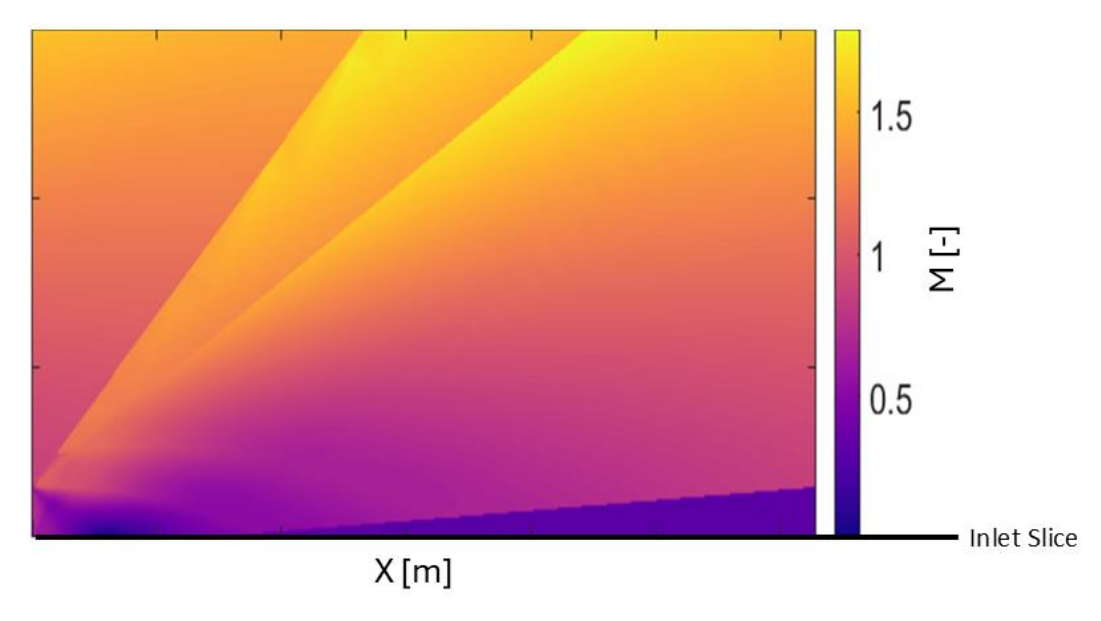


Figure 4: MOC Model Mach Contour

The simulations were run over approximately 24 wave cycles to ensure that the solution converged. The simulations were considered converged when a clear repetition of low frequency oscillations that are present in the system are shown. This convergence is represented by the mass flow values output from CFD++ and a moving mean performed over 10 full wave cycles. This is demonstrated in Figure 5.

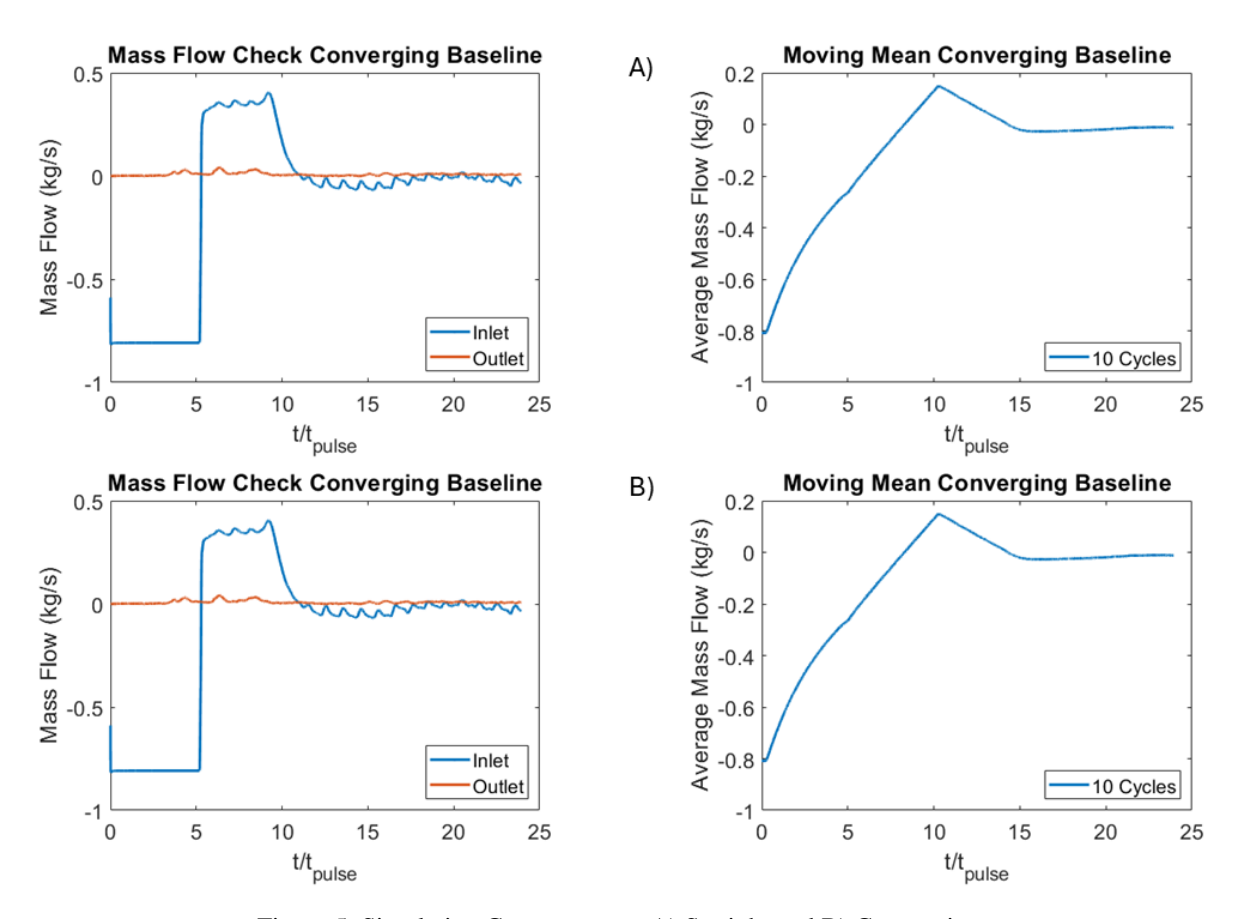


Figure 5: Simulation Convergences: A) Straight and B) Converging

The straight baseline was also run for a total of 60 wave cycles to determine when convergence occurred to avoid running the simulations for excessive periods of time. This is demonstrated in Figure 6 below.

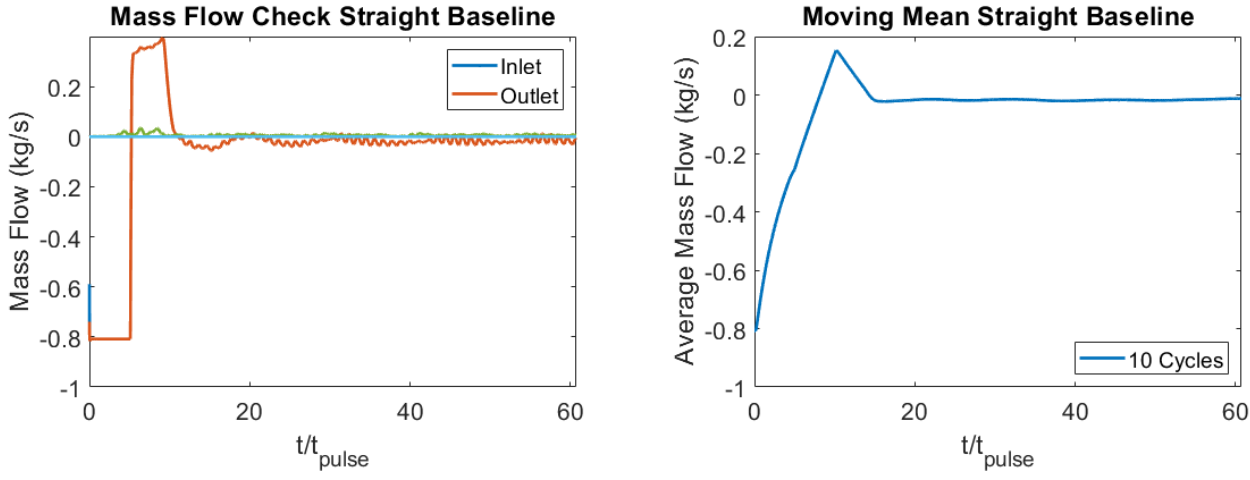


Figure 6: Straight Baseline Full Convergence

# **B.** Injector Performance Parameters

A number of different parameters were obtained to characterize the individual performance of an injector. Some of these parameters include the steady/unsteady  $C_D$ , the percent obstruction, and the average mass flux in. The steady  $C_D$  is an important parameter to consider as it is a measure of the efficiency of the injector. It is a ratio of the actual

mass flow rate coming from the injector compared to the ideal mass flow that is projected for an injector with similar geometry. C<sub>D</sub> calculations are shown in Eqns. 1-2.

$$\dot{m}_{ideal} = \frac{AP_0}{T_0} \sqrt{\frac{\gamma}{R}} \left(\frac{\gamma + 1}{2}\right)^{-\frac{\gamma + 1}{2(\gamma - 1)}}$$

$$C_D = \frac{\dot{m}_{actual}}{\dot{m}_{ideal}}$$
 2

The  $C_D$  equation is also used to obtain the average unsteady  $C_D$  of the unsteady cases. This is the discharge coefficient over time averaged per cycle. The average is taken over 10 cycles as the low frequency oscillations that occur within the domain have a frequency of about 10 cycles. The others throughout this paper were taken in a similar fashion.

Another parameter that was used to analyze the performance of these injectors is injector stiffness or  $\frac{dP}{P}$ . Injector stiffness is an important parameter to consider in injectors due to the effects it can have on injector performance and combustion efficiency. Injector stiffness influences combustion stability, injector mixing, and overall effectiveness [12]. The definition of injector stiffness for these simulations is shown in Eqn. 3.

$$\frac{dP}{P} = \frac{P_{feed} - P_{chamber}}{P_{chamber}}$$

Where  $P_{\text{feed}}$  is the pressure from the left boundary condition that drives the flow and  $P_{\text{chamber}}$  is the average pressure of the chamber on the injection plane. A diagram of this is shown below.

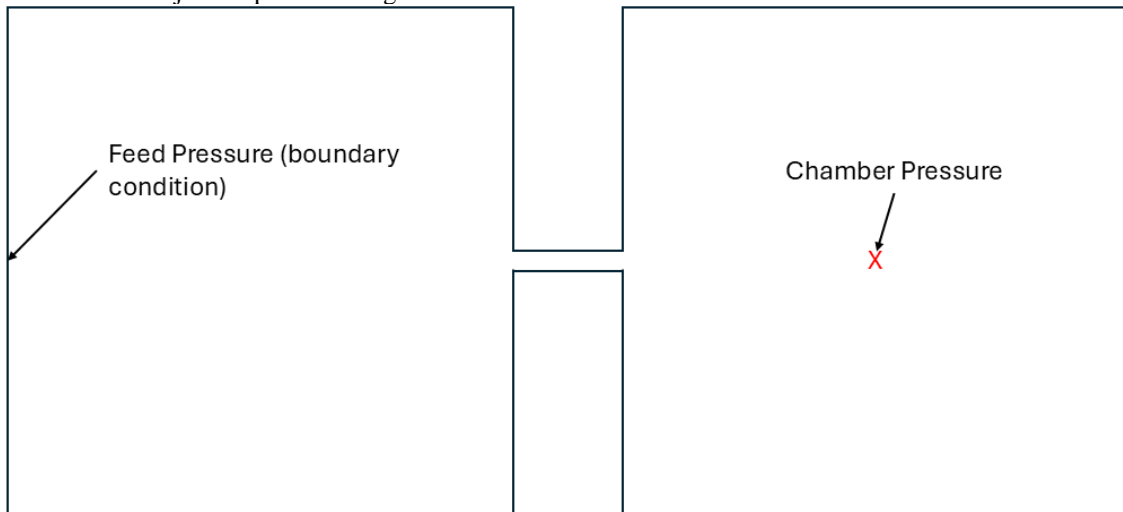


Figure 7: Injector Stiffness Definitions Diagram

Some other important parameters that were also considered include the average mass flux, average percent time obstructed, and the pressure attenuation. The average mass flux is achieved through dividing the total mass injected into the chamber by the cross-sectional area of the of the outlet of the injector as shown in Eqn. 4. This is to compare different size injectors to each other. By dividing out the area of the injector it removes the dependence of the amount of mass injected on the actual diameter of the injector.

$$q = \frac{\int_{y_1}^{y} \int_{t_1}^{t_2} \rho V dt dy}{A}$$

The average percentage time obstructed indicates how long the injector stops injecting fuel in a detonation wave cycle. This is determined based off 'color trace' data obtained in Tecplot. The detonation wave fluid is indicated as a color trace of 1 and the injected fluid is indicated as a color trace of 0. If the flow at the outlet of the injector has a color of above 0.5 it is blocked. This relates to the recovery of the injector as it also tells how long it takes for the injector to start injecting fuel and/or oxidizer again. Finally, the pressure attenuation shows how the pressure changes as the wave

travels back through the injector, namely how much the pressure reduces as it travels back through the injector. Ideally, the inlet will experience as little pressure fluctuation as possible to avoid any issues with injection and any system upstream of the injector.

#### C. 2D Method with Chemistry

One of the biggest challenges with single injector analysis is determining if decoupling of the chemistry is a good approximation. One way of coupling combustion and full-scale effects while also balancing the computational cost is with unwrapped two-dimensional simulations. Figure 8 shows the boundary conditions for the 2D method with chemistry.

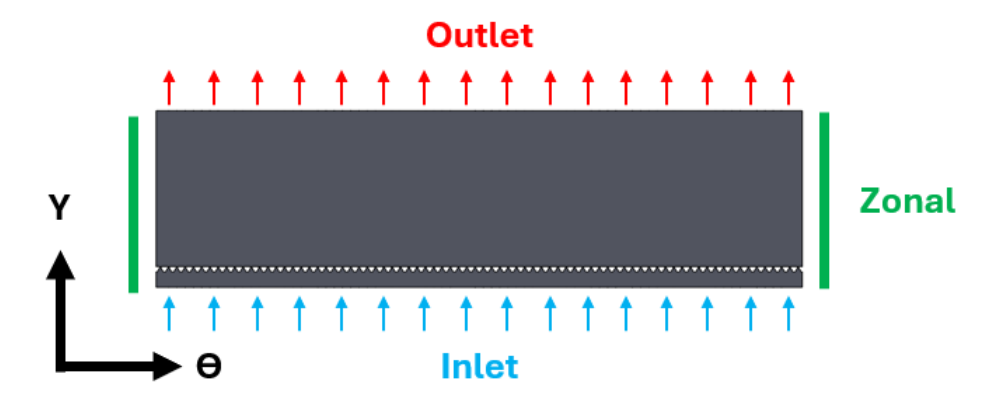


Figure 8 2D Reactive Boundary Conditions

Figure 8 shows the boundary conditions for the 2D method with chemistry. The mesh was generated with Fidelity Pointwise and simulated with Metacomp ICFD++. The distance from left to right in Figure 8 is the circumferential distance around the combustor, in terms of distance travelled or angle from start. The vertical distance is the distance down the RDE, going from injection at the bottom to the outlet at the top. The inlet is a total pressure boundary condition that is imposed at 5 Bar. The outlet is a static exit boundary condition in which the outflow can switch from subsonic to supersonic with varying pressure. The pressure at the outlet is computed based on the flow next to the boundary condition and changes with time as the system changes. The two zonal boundary conditions are used for connections between cells that are imposed by location, rather by direct cell-to-cell connections through faces in the mesh. This means flow can move into one zonal boundary condition and go out of another without the mesh physically connecting the two. For the 2D method with chemistry, flow can freely travel between each side of the combustion chamber and injection plenum. This results in the periodic rotating detonation seen in the RDE. A simple, one step reaction mechanism is introduced to combust a premixed hydrogen oxygen mixture.

$$2H_2 + O_2 \rightarrow 2H_2O$$
 5

This one step reaction chemistry has been used in previous premixed RDE simulations for simulating detonation waves [13-14]. The process for starting an unwrapped simulation is as follows. Firstly, reactants are imposed until a steady state point is reached. This will be referenced throughout the text as a cold flow simulation. Once a steady cold flow solution is found, a hot spot is imposed in the combustion chamber. This hot spot causes the premixed reactants in the combustion chamber to detonate and spawn one or more waves. The simulation takes time to reach a quasi-steady state where a finite number of detonations waves are found and not changing.

The performance variables defined above are utilized for single injector schemes. The unwrapped work simulates the full system; therefore, other performance metrics need to be considered as well. Firstly, pressure gain is defined below.

$$P_{Gain} = \frac{P_{Out} - P_{In}}{P_{In}} \tag{6}$$

Pressure gain is the measure of imposed inlet pressure versus the amount of pressure leaving the system. The pressure in is the imposed total pressure inlet boundary condition, and the pressure out is the total pressure leaving the system. Pressure gain is of particular importance for a pressure gain combustion (PGC) system such as an RDE. Also important

is the thrust of the system, which is measured by the mass and pressure force leaving the system out of the outlet. The thrust is expected to reach a constant value in time to show the system has reached a quasi-steady state.

## III. Results

# A. 2D Results without chemistry

The straight baseline injector was the first injector that was tested with the computational method without chemistry. It was also tested under steady conditions to obtain the steady  $C_D$  to compare to unsteady results. In Figure 9, the fully developed flow contours are shown comparing the steady and the unsteady flow.

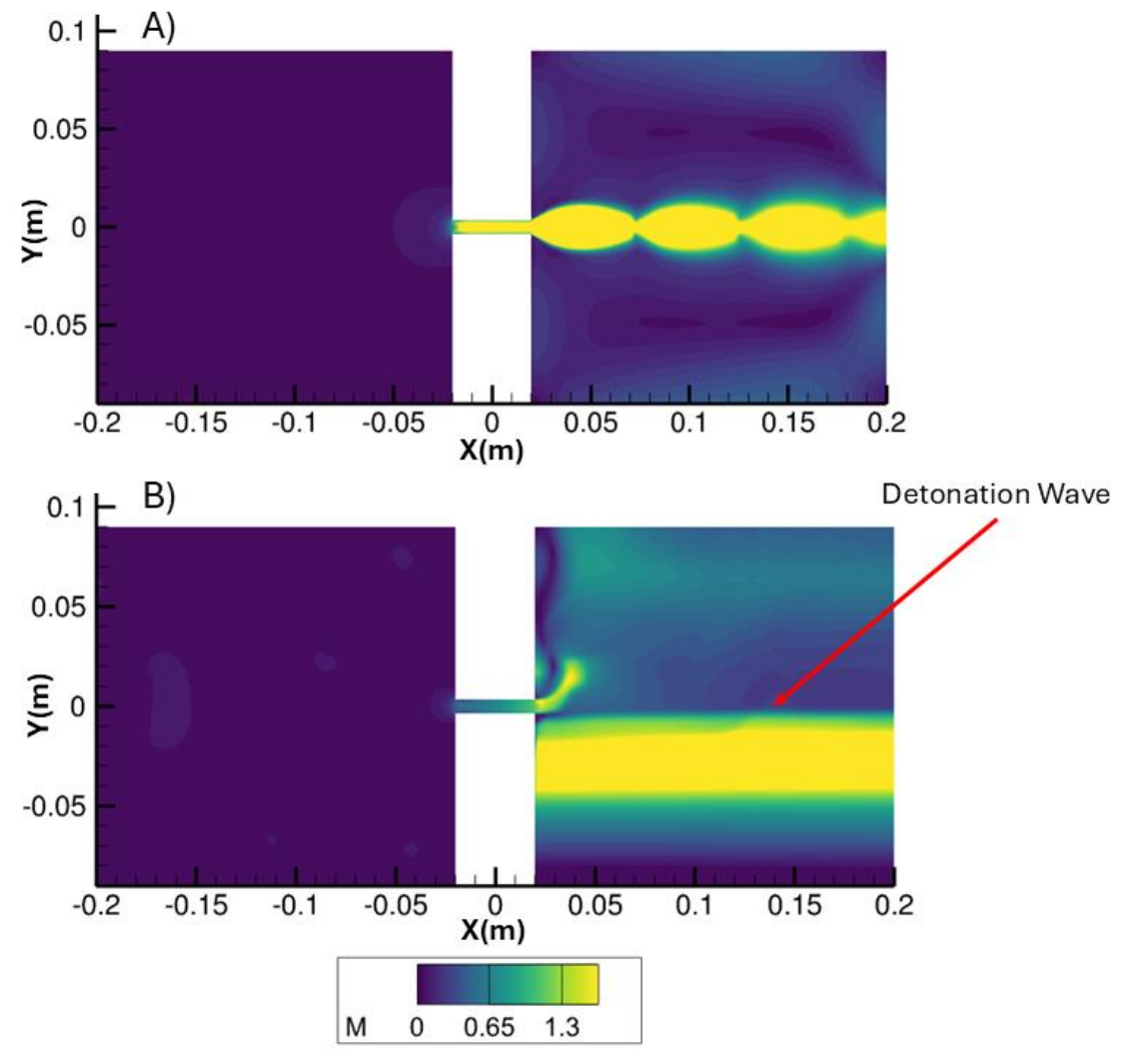


Figure 9: Fully developed Mach number contours A) Steady Flow B) Unsteady Flow

From the steady flow, it was found that the steady  $C_D$  was 0.83. After the straight tube was developed and simulated, a baseline geometry with a converging inlet was created to reduce inefficiencies created by the abrupt transition into the injector in the straight tube geometry. One of those inefficiencies is a vena contractra, shown in Figure 10, that is formed in the inlet of the straight baseline. This reduces the overall performance of the injector, reducing the  $C_D$  and the mass injected, and is a well-studied phenomenon [15].

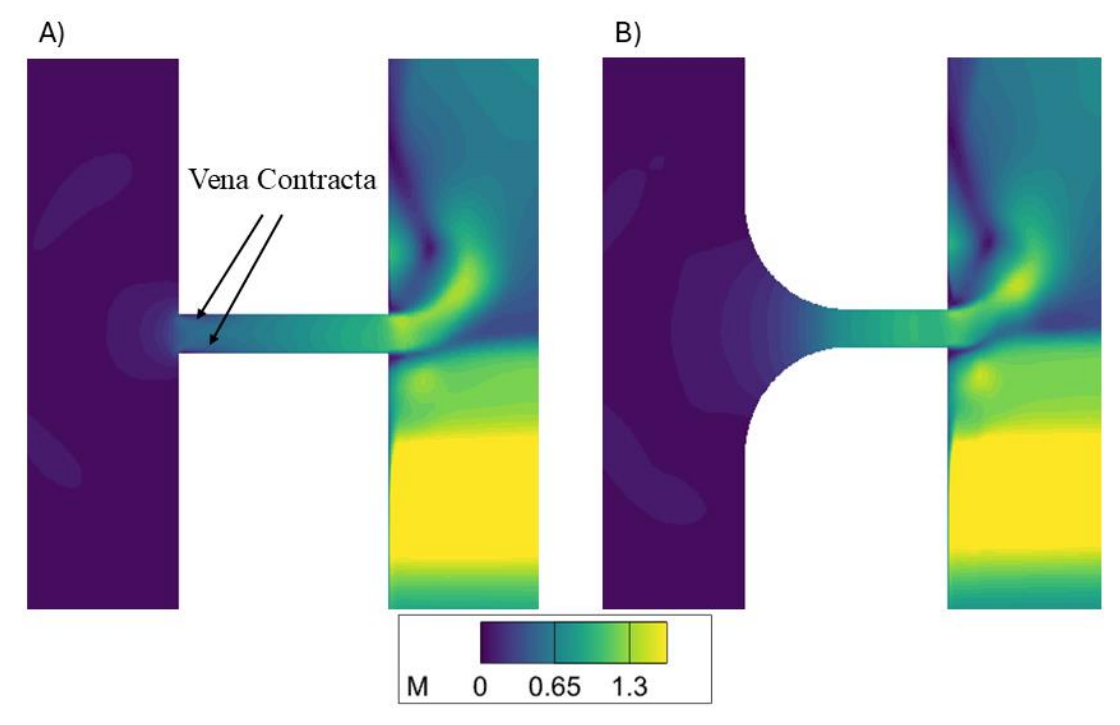


Figure 10: Vena Contracta in Straight Tube Baseline A) Straight Baseline B) Converging Baseline The results comparing the two baseline cases are outlined in Table 1.

Table 1 Straight Baseline vs Converging Baseline Performance without chemistry at 10 Bar feed pressure

Case	Steady cold flow C <sub>D</sub>	Average Hot flow C <sub>D</sub>	Hot flow/cold- flow cd	Average % Time Obstructed	Average Mass Flux Injected (g/m^2)
Straight	0.82	0.38	0.46	22.0%	165.2
Converging	0.93	0.43	0.46	16.2%	191.7

From the results outlined above, the converging baseline geometry performs better in all the pertinent performance parameters. The hot flow-over-cold-flow discharge of 0.46 demonstrates that both geometries perform equal under the unsteady pulse conditions which is consistent with findings in Lim, et al. [16]. The straight baseline was also done at 6 and 8 bar feed total pressures to see how injector stiffness effects the performance of the injector. Flow profiles are made from 200 data points captured across the centerline of the domain, at the inlet of the injectors, and at the outlet of the injector. These points are captured every 5 timesteps and the last 10 cycles are taken to perform calculations with. The profiles are created with the last 3 cycles to make it easier to distinguish flow characteristics. With these profiles we can see how the flow behaves at each of these three locations. Figure 11 displays centerline profiles for both the straight and converging baseline cases. From these profiles the wave speed and the reduced frequency can be found. The equation used to calculate the reduced frequency is defined below in Eqn. 7.

plate the reduced frequency is defined below in Eqn. 7. 
$$f_r = \frac{f_w}{U_{inj}/L}$$

Where  $f_r$  is the reduced frequency,  $f_w$  is the wave frequency,  $U_{inj}$  is the velocity of the wave travelling back through the injector, and L is the length of the injector. The results of this are recorded in Table 2. The reduced frequency is below one, demonstrating a relatively low speed throughout the injector compared to the excitation frequency.

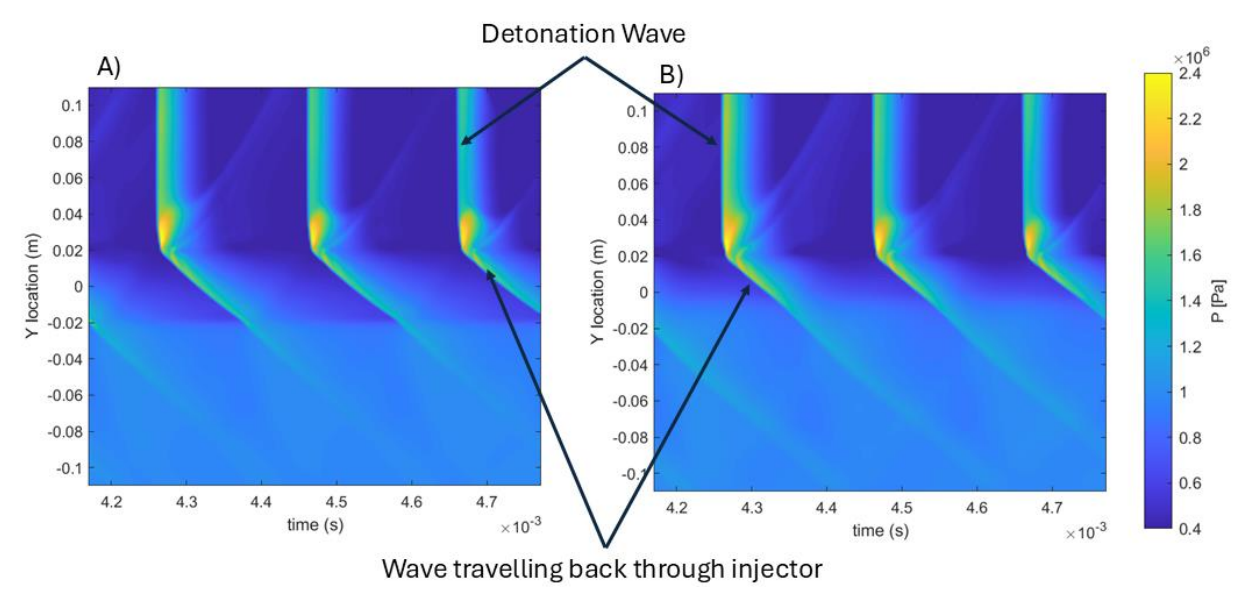


Figure 11: Centerline Pressure profiles for standard size baseline geometries A) Straight B) Converging

The momentum profiles at the outlet of the injector were also taken to characterize the flow and demonstrate when reversed flow is present. This is plotted in Figure 12. The black lines indicate where the momentum is 0 while the areas within the black lines indicate where the momentum is negative. The negative momentum indicates that the flow is reversed in those areas.

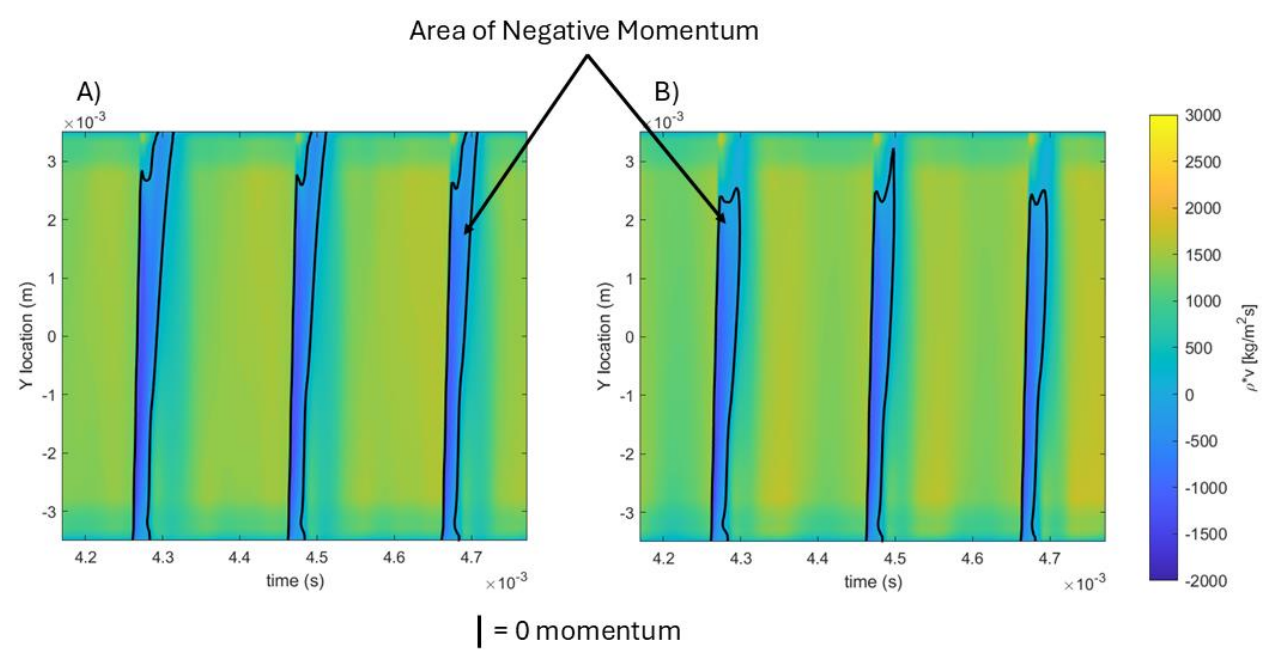


Figure 12: Outlet Momentum Profiles over time A) Straight B) Converging

The straight baseline geometry experiences full back flow at the outlet of the injector throughout the diameter of the injector while the converging baseline has full forward flow toward the top of the injector. This could be due to the increased performance of the injector caused by the reduction of the vena contracta. The stoppages in both injectors have similar overall characteristics with an extended period of forward flow toward the top of the stoppage and quicker recovery toward the bottom of the injector (indicated by a thinner period of reversed flow). In Figure 13 and Figure

14 the time evolution of the flow in the converging baseline injector is shown. Figure 13 plots synthetic schlieren images from the flow. In these, the line of pressure gradients can be clearly seen. In Figure 13a the gradients from the injection flow are shown coming out of the outlet of the injector as well as the incoming detonation wave. There is also a lighter area below the detonation wave that is caused by the viscous wall. In Figure 13c the detonation wave can be seen striking the injection flow, creating two distinct lines. The lower line is the detonation wave while the upper line is the injection flow being pushed back into the injector by the wave. Finally, in Figure 13e and f the resulting pressure wave from the detonation wave is seen starting to travel back through the injector and the obstructed flow is seen at the outlet of the injector. Figure 14 plots the Mach contours over time with similar points of interest outlined.

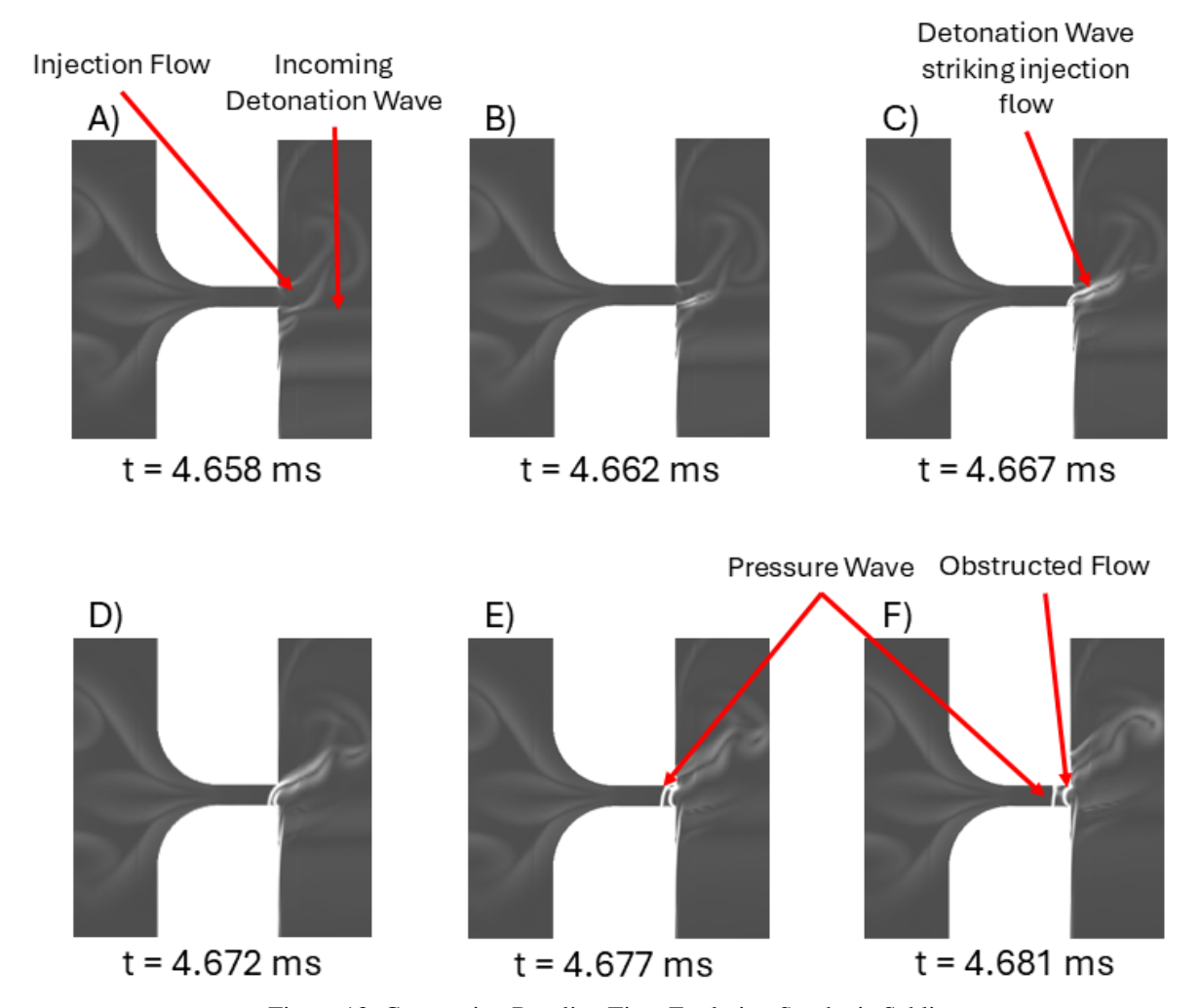


Figure 13: Converging Baseline Time Evolution Synthetic Schlieren

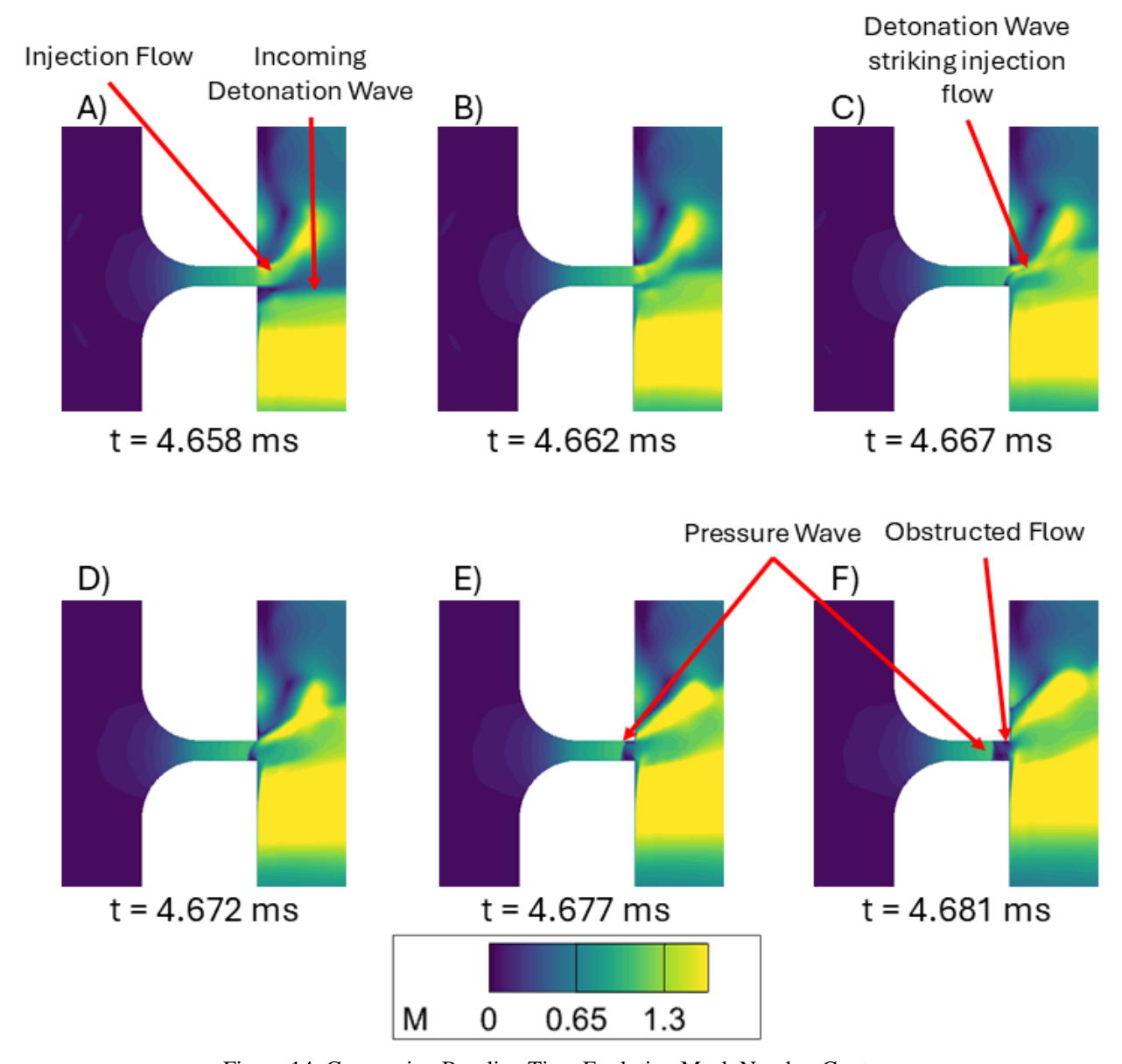


Figure 14: Converging Baseline Time Evolution Mach Number Contour

Figure 15 shows the pressure attenuation in both the converging and straight geometry. At points, shown in Figure 16, along the length of the injector the static pressure is tracked to determine how the pressure dissipates as the pressure wave travels back through the injector. In the converging injector, while the pressures are slightly higher entering the injector by the time the wave reaches the inlet of the injector the pressure has reduced drastically compared to the straight injector. For both injectors, by the time they reach the center of the inlet plenum it has almost leveled out to the inlet boundary condition, in this case, 10 bar. From this, the percentage difference between the center of the injector and the inlet of the injector was taken. It was found that that the pressure decreased by 29.5% in the converging baseline while in the straight tube baseline decreased by 15.3%. However, the percentage difference at the inlet plenum compared to the feed pressure for the straight baseline is 4.83%, while the percentage difference for the converging geometry is 10.0%. This indicates higher pressure attenuation within the injector but not as much dissipation as it enters the inlet plenum.

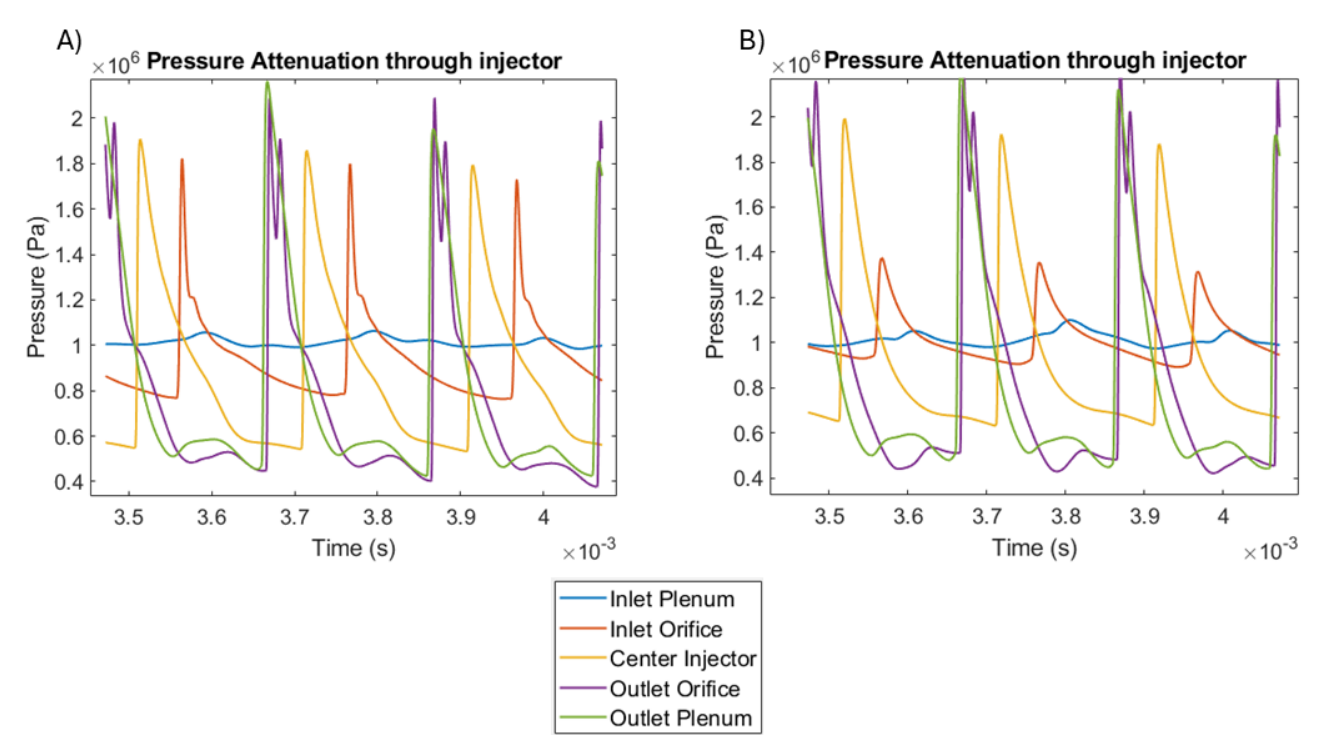


Figure 15 Pressure Attenuation Throughout the Length of the Injector A) Straight B) Converging

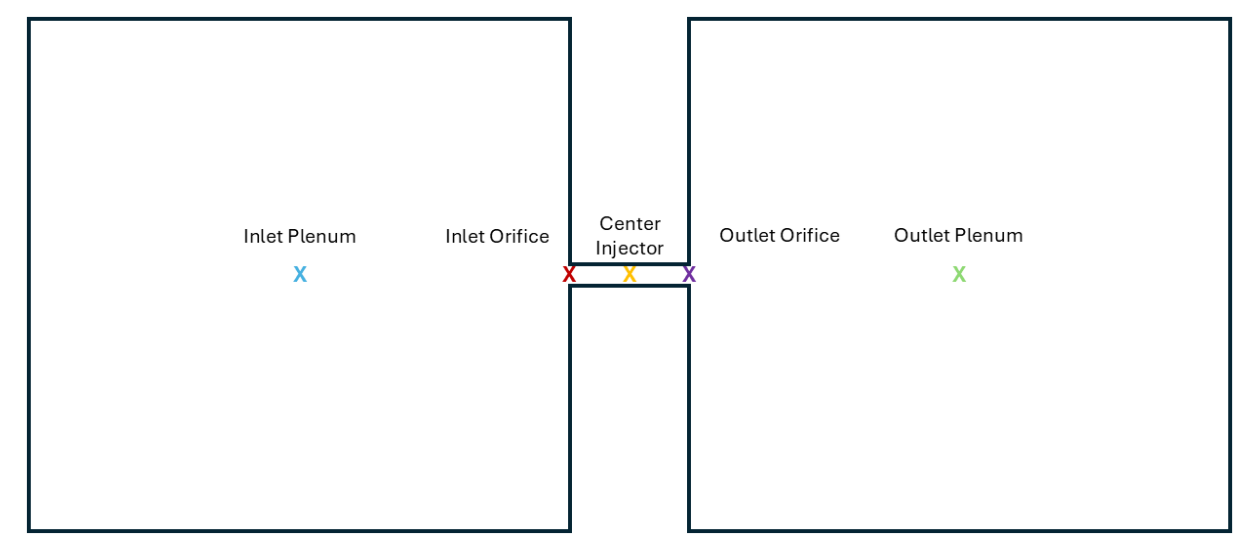


Figure 16 Node Locations for Pressure Attenuation

Finally, a set of simulations of the straight baseline was done at different feed total pressure to determine the effect of injector stiffness on the performance of the injector. These results are outlined below in Table 2. Additionally, the theoretical blockage is calculated, which is defined as the amount of time the feed pressure is below the pulse pressure.

Table 2 Straight Baseline Injector Stiffness Study Results

Feed Pressure (Bar)	Injector Stiffness	Theoretical blockage (%)	Reduced Frequency	Average % Time Obstructed based on U Velocity	Average % Time Obstructed	Average Mass Flux Injected
				•	based on Color	(g/m^2)
					Trace	

6	-0.175	49.4	0.327	33.2	81.2	3.880
8	0.098	33.3	0.390	14.0	15.4	91.69
10	0.420	13.5	0.613	12.0	22.0	171.74

These results depict that, as the stiffness metric increases, the overall performance of the injector improves. The unsteady  $C_d$  evolution over 3 cycles for the 6 bar case and the 10 bar case is depicted below in Figure 18. The average steady  $C_d$  is never obtained for any of the cases and the  $C_d$  for the 10 bar reaches a higher maximum over the course of a cycle. This contributes to its higher overall performance. Also included in Table 2 above is the theoretical percent blockage. This is taken by calculating the amount of time the pressure crossing the injector is above the feed pressure. An example of this is shown below in Figure 17.

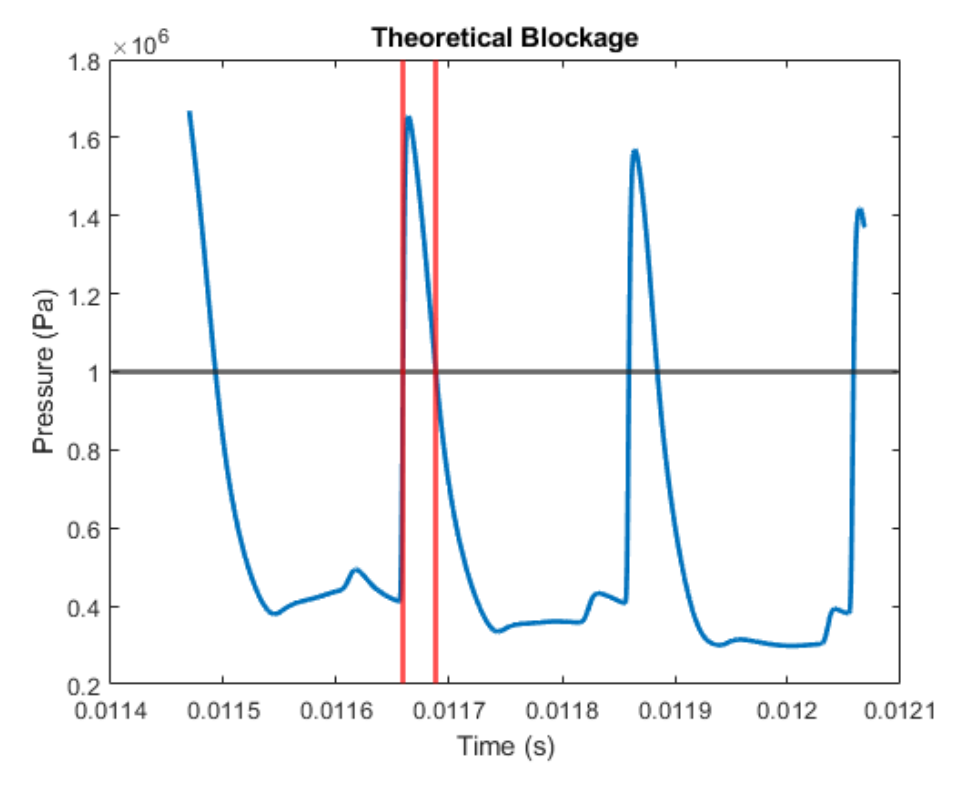


Figure 17: Theoretical Blockage Diagram

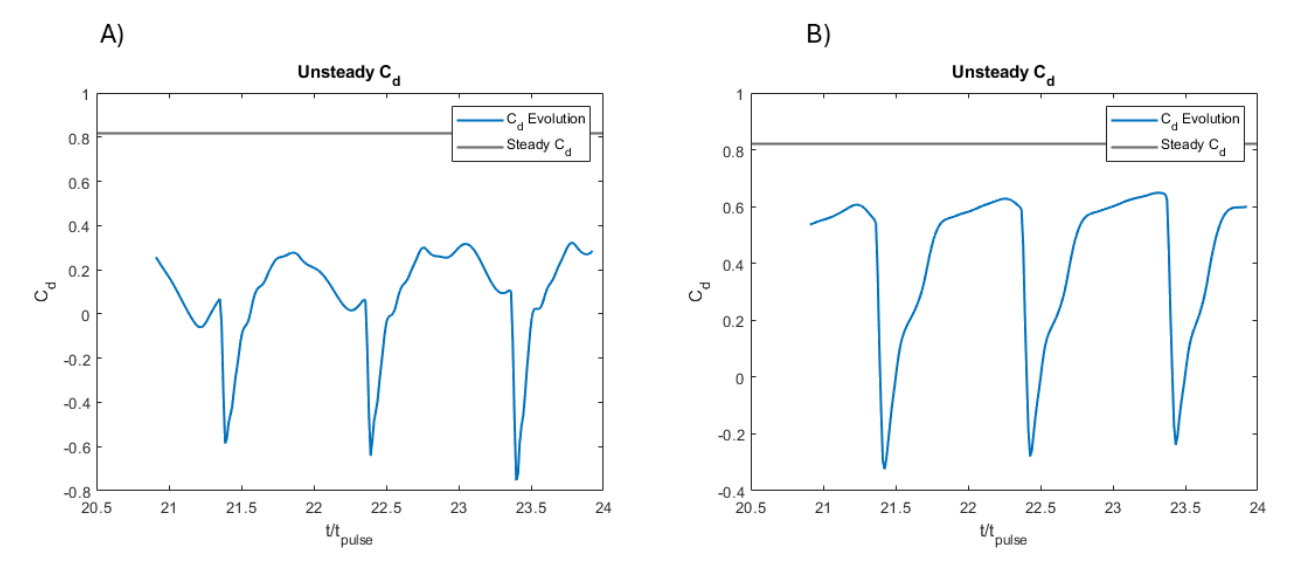


Figure 18 Cd Evolution for different injector stiffnesses: A) dP/P of -0.175 and B) dP/P of 0.42

#### **B. 2D Reactive Results**

The converging baseline geometry was simulated with the 2D reactive method. An example contour of the Mach number is shown.

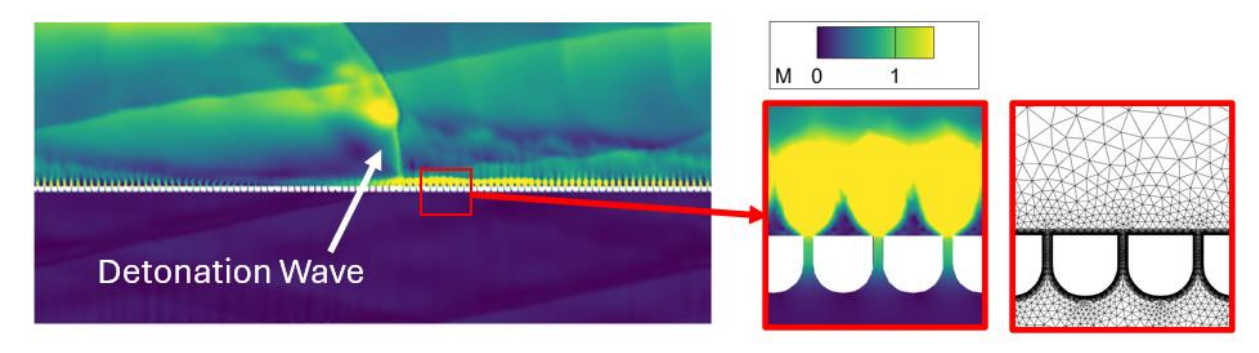


Figure 19 Mach Contour of 2D Reactive Simulation of Converging Baseline

For the unwrapped simulation, the case steadied itself to one detonation wave, depicted in Figure 19. A zoomed image of the Mach number and mesh for three injectors is also shown. Mach number is of particular interest, as lower Mach number injection would improve mixing of the reactants. To prove the case has reached a quasi-steady state, multiple metrics are plotted. These are recorded in Fig. Figure 20.

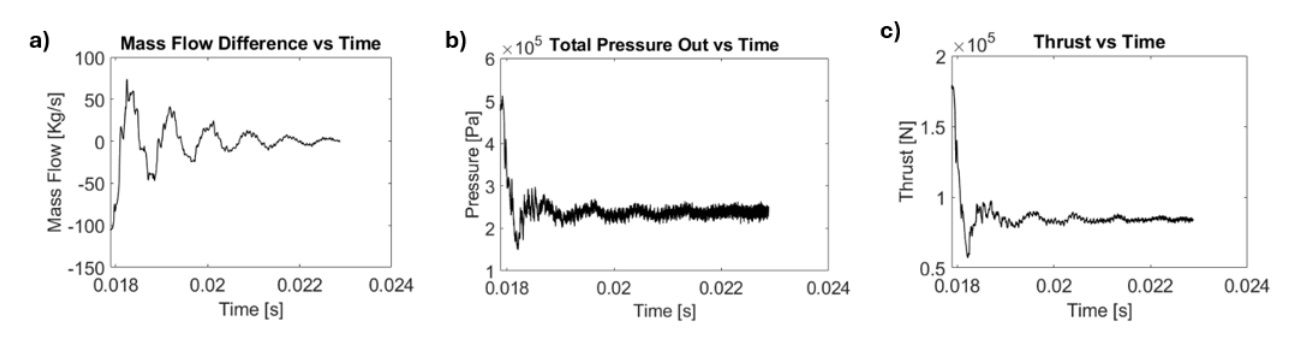


Figure 20 a) Mass Flow Difference b) Total Pressure c) Thrust all over time

Figure 20a plots the difference between inlet and outlet mass flows. Due to the pressure-imposed inlet and outlet boundaries, the mass flow has to approach a single value to come in and out of the system. If the case is truly converged, the value the difference in mass flows is approaching should be zero, as mass would not be lost or generated throughout the process. Figure 20a visualizes this, as well as the trend approaching a steady value, therefore, the mass flow is considered steady. Figure 20b and c plots the total pressure and thrust leaving the system, respectively. These plots outline how the total pressure and thrust approaching a single value, albeit with some noise due to the unsteadiness of the simulation. Other performance metrics for the unwrapped simulation are defined in the table below.

Table 3: Unwrapped Converging Baseline Performance Metrics

Unsteady CD [-]	Detonation Wave Frequency [kHz]	Detonation Wave Speed [m/s]	CJ Speed [m/s]	Pressure Gain [-]	DP/P [-]	Thrust [N/m]
0.67	4.6	1900	~1960	-0.51	1.8	8.5E+4

The unsteady CD is the discharge coefficient for the whole system, not just a single injector. This can be calculated with Eqn. 1 and Eqn. 2, with small modifications to change from the single injector scheme to the fully unwrapped case. Firstly, the area in the mass flow rate equation is changed to be the total choked area of the unwrapped simulation. This is calculated by measuring the throat of one injector and multiplying by the number of injectors. The other metric that changes is the specific heat ratio. The resulting value is unsteady in time but approaches a single value alike the metrics previously shown and is plotted in Figure 21d.

The detonation wave frequency was calculated using the peaks of the detonation wave over time, and an FFT of the detonation wave. A node was placed inside the combustion chamber where the detonation wave traveled through, and data was collected at this point over time. The pressure trace collected here is plotted in Fig. 20.

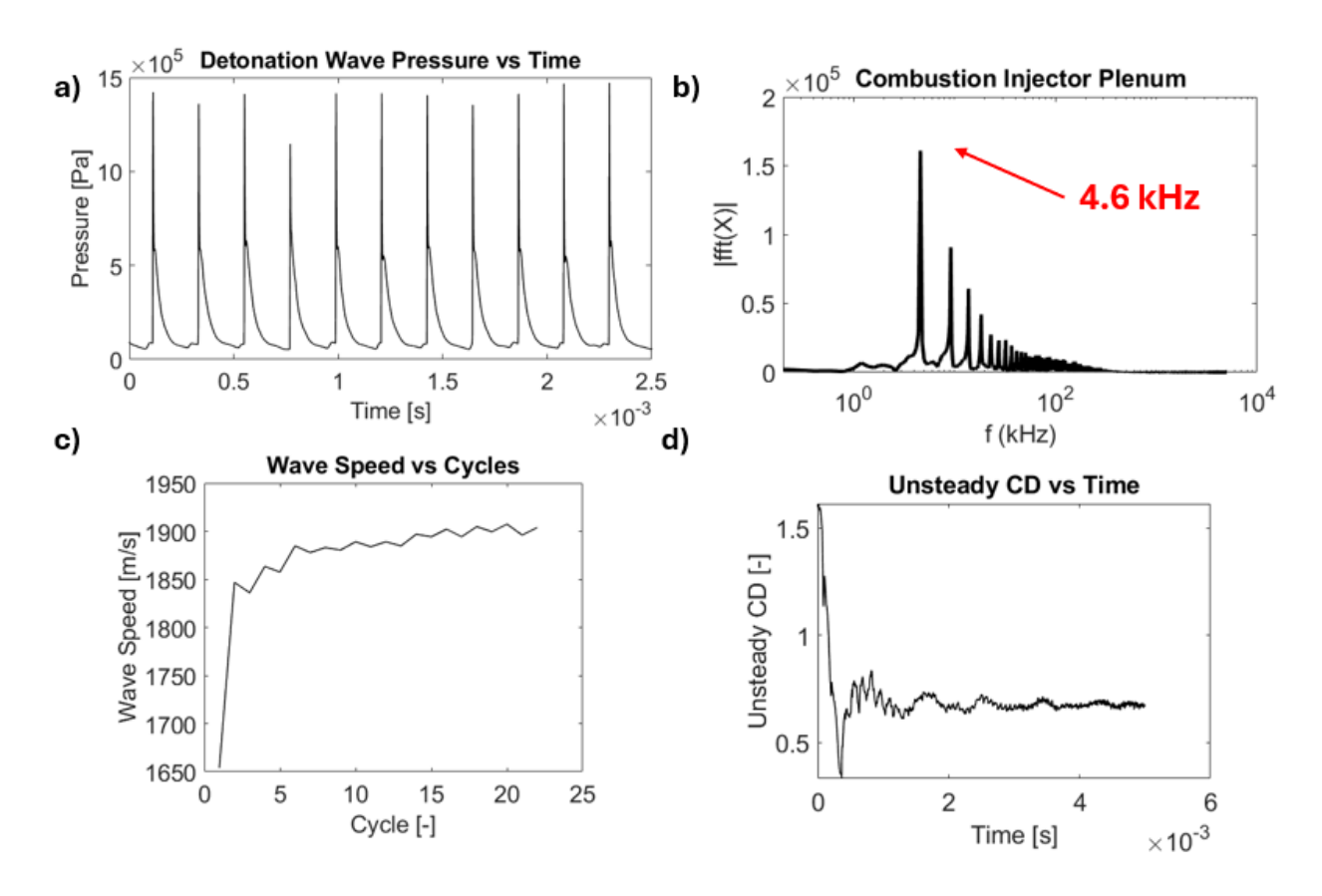


Figure 21 a) Node Pressure in Combustion Chamber b) Node Pressure FFT c) Wave Speed d) Unsteady CD all over multiple cycles

The spikes in Figure 21a represent the detonation wave passing over the node through time. Tracking the time at which each peak value occurs, and calculating how frequent this occurs is one way frequency was achieved. The other method is taking an FFT of the same data which reaches a value of 4.6 kHz, aligning exactly with the peaks method. Figure 21c depicts the wave speed over cycles of the detonation wave as it steadies out to a constant wave speed. The wave speed approaches the Chapman-Jouguet (CJ) speed but converges at about 3% below the CJ speed [14].

The pressure gain in Table 3 is negative as the total pressure out does not reach values above injection pressure. Figure 20b plots the value total pressure out of the system is approaching, about 2.5 Bar. The DP/P is calculated the same way as the single injector, with chamber pressure being defined as average pressure of the node in the combustion chamber.

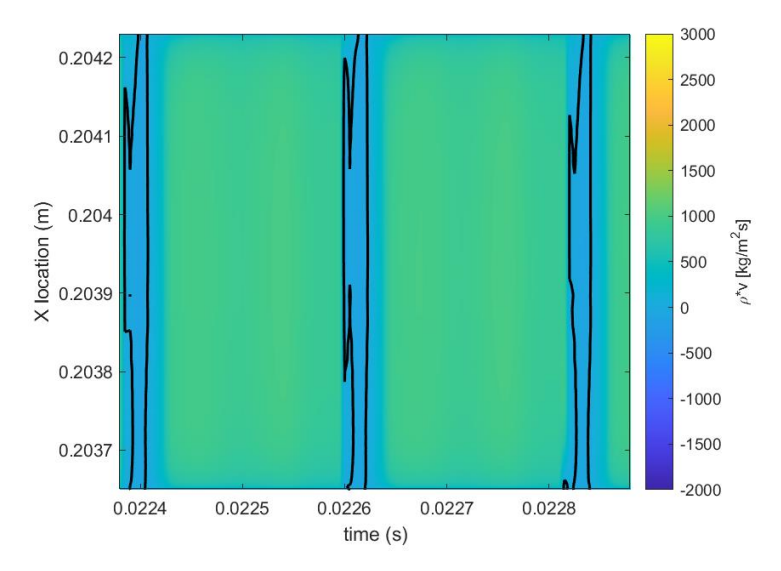


Figure 22 Momentum in Time for a Single Converging Injector for 2D Unwrapped Method

Figure 22 depicts the same momentum contour in time for a single converging injector; however, this result comes from plotting one injector in the 2D unwrapped scheme. The data can be compared with Figure 12b where the left axis depicts the position of the data, the bottom axis records the step in time, and the right axis visualizes the contour level of the data. The entire unwrapped RDE is simulated, and a line of data is taken across the exit of one of the injectors. The regions of backflow, the area enclosed in black lines, match the results in Figure 12b in both position and time. Similarly, the magnitude of constant injection has a roughly 15% difference, while also matching position and time.

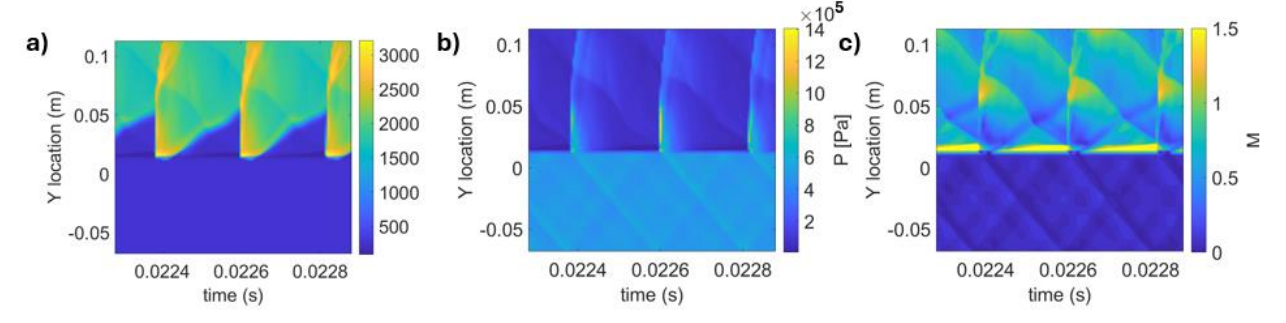


Figure 23 a) Temperature b) Static Pressure c) Mach Number Through the 2D Unwrapped Converging Tube in Time

Figure 23 plots the centerline contour method used for the single injector scheme in the 2D unwrapped case. The line of data exists from inlet to outlet and passes through the center of one converging tube injector. The left axis changes to be the inlet at the bottom, injection just after zero, and exits at the top of the image. Figure 23a records the temperature, which clearly defines the refill region grow and get consumed as each detonation wave passes. This could be used as a method of penetration depth to calculate how far and how fast reactants are being injected into the combustion chamber. Figure 23b and c plot the static pressure and Mach number, respectively. Figure 23b can be compared with Fig.Figure 11b as they both plot the centerline pressure. Both plots visualize the detonation wave and the corresponding propagating wave travelling upstream into the injection region. Figure 23c allows the visualization of when the injectors reach a local steady injection rate. This occurs when the Mach number after the detonation wave passes reaches a steady value. This could be used as a different method of recovery rate to compare injector geometries and cases.

## IV. Validation

# A. Testing Platform and Injector Response

Rotating Detonation Engines are a highly coupled system in which minor changes to the injection scheme can have a cascade of effects on other areas of the combustor [17]. This makes corelating injector performance to overall engine performance challenging. To experimentally isolate injector performance from engine performance, the injector problem is decoupled into a detonation driver and a single element injector (SEI). An RDC is utilized as the detonation driver and provides a consistent downstream boundary condition for injector evaluation. The SEI is inserted into the RDC environment and operates at conditions that do not disturb the detonation driver. This creates a one-way coupled system in which injector performance is isolated to only be a function of the injector operating conditions. This technique has been described by Hoeper et. al [18].

The RDC test platform and its design have been detailed in prior work [19] A brief description is provided here for continuity. The RDC, THOR, is shown in the configuration used in Figure 24. The RDC is fueled by a hydrogen-air mixture and injected into the detonation channel in a jet-in-crossflow (JICF) design. Air is injected through a converging diverging slot with a throat gap of 1.42mm. The flow expands to an area ratio of 1.18 where gaseous hydrogen is then injected through 100 discrete orifices. The flow continues to expand to an area ratio of 1.81, then reaches a backward-facing step (BFS) with an expansion ratio of  $\sim$ 7 into the detonation channel. The detonation channel has a diameter of 136 mm, and a width of 10.7 mm. Sonic nozzles are used to meter the air and gaseous hydrogen with an uncertainty of  $\sim$ 2% of the flow rate. THOR is initiated using a  $H_2/O_2$  pre-detonator. To maintain a consistent detonation driver, all tests are conducted at a total flow rate of 1 lbm/s and an equivalence ratio of 1. A quartz outer body is used to provide optical access to the detonation channel.

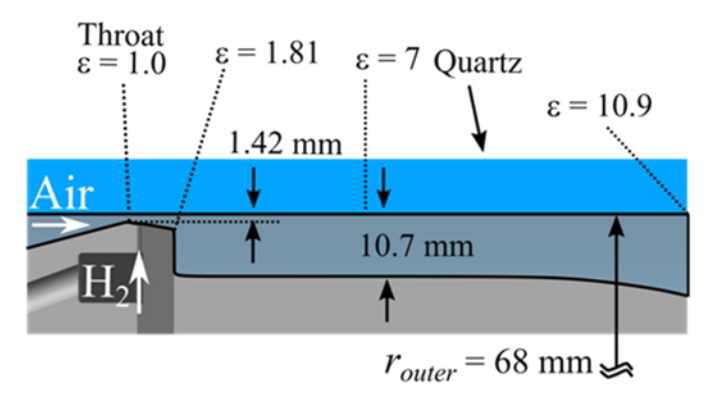


Figure 24: Cross section view of THOR (reprinted from [20] with permission from the authors).

The SEI layout can be seen in Fig.Figure 25. Three hydrogen orifices are removed from the fuel injection to allow for the SEI to fit into the hardware. The SEI injects directly into the channel from the BFS. CTAP pressure measurements are made at the same location on the BFS clocked at 67.5 degrees in the positive and negative azimuthal direction to quantify the time averaged downstream conditions. The manifold geometry of the SEI can be seen in Figure 25. The SEI injection system consists of large manifolds located ~1.25" away from the injector orifice. CTAP measurements are made inside the manifold to quantify the injector's upstream conditions. The flow path between the injector orifice and the manifold has a minimum area that is ~5 times bigger than the orifice to ensure minimal pressure loss.

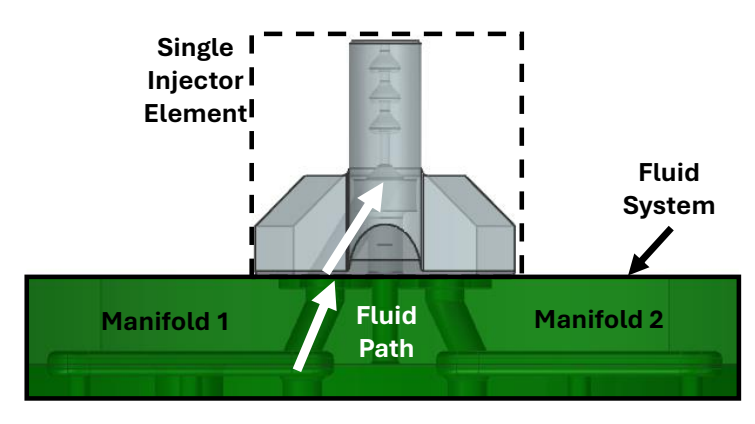


Figure 25: Fluid paths for the SEI system.

Discharge coefficients are determined for injector stiffness values ranging from  $\sim 0.5$  to 1.5. Nitrogen is used as a surrogate gas for evaluating injectors. The fluid systems are described as follows. Nitrogen is metered through a computer-controlled regulator to control the pressure upstream of a sonic venturi. The sonic venturi is maintained at a choked condition to ensure constant mass flow to the test article. During testing operations, the pressure is set upstream of the venturi and the run valve is opened to allow for flow to the test article. Once the gas reaches a steady state, the detonation driver is primed with reactants and ignited using the pre-detonator. The CTAP pressures, locations described above, are collected throughout the test to determine the average upstream and downstream conditions throughout the test. Discharge coefficients are also calculated live throughout the test. An example of the pressure traces and  $C_d$  value can be seen in Figure 26.

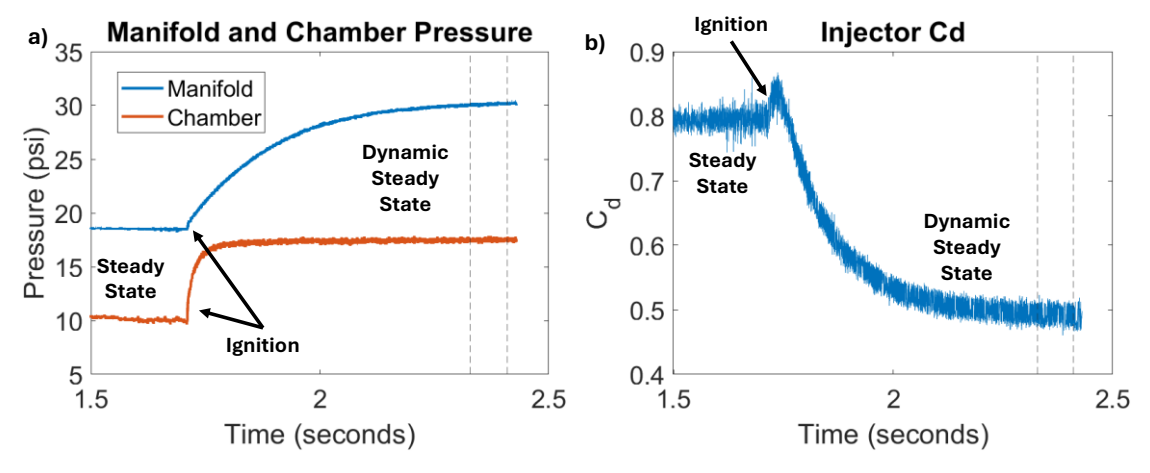


Figure 26 Experimental a) manifold and chamber pressure trace b) discharge coefficient

During testing operations, the cold reactants and injector surrogate fluid are flowed until they all reach a steady state. This initial phase is used to collect steady state measurements of the injector performance. The cold reactants are then ignited causing an abrupt change in the chamber pressure. To account for this change, the injector manifold pressure also rises until it reaches a new dynamic steady state. The unsteady  $C_d$  is calculated during the dynamic steady state for a variety of injector stiffnesses.

### **B.** CFD and Experimental Comparison

Two experimental testing campaigns were conducted using straight tube and converging baseline injectors alike those simulated in the CFD. The average unsteady CD can be calculated experimentally using venturi mass flow data to compare with CFD of the same case. The results are plotted in Figure 27.

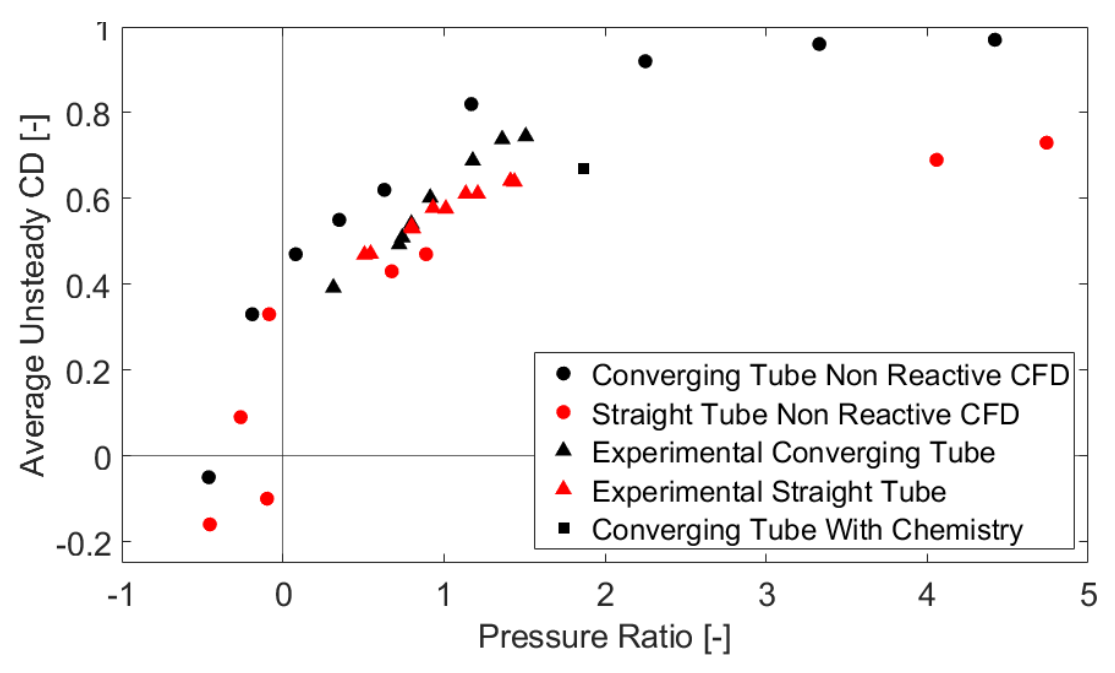


Figure 27 CFD and Experimental Average hot flow CD

Figure 27 visualizes a correlation between the experimentally found average unsteady CDs with the CDs found in the CFD. The circles are CFD nonreactive simulations, the square is from the 2D unwrapped simulation, and the triangles are from experimental test campaigns. The black data is from the converging tube, and the red data is from the straight tube. The converging baseline CFD and experiment correlate along the same trends with discrepancies below 18% for the CFD vs the experiment. Similarly, the straight tube CFD and experiment seem to follow the same trend as each other, while both being either the same or slightly worse than the converging tube, which agrees with the single injector conclusions. Finally, the 2D Unwrapped converging baseline is plotted and follows the same stiffness-to-unsteady-cd trends, confirming that the non-chemistry approach can be used to mimic detonation-like injectors. A discrepancy between the case with chemistry and without chemistry can be due to the imposed pulse having a different profile than the detonation wave. The metric to measure the pulse strength is defined as the difference in maximum and minimum pressure, divided by the pulse average pressure. This is how different detonation waves can be considered with how they impact the injector. The nonreactive pulse strength results in a value of 1.1, and the reactive detonation wave strength calculates to 8.1. The higher this number is, the stronger the pulse is influencing the injector. Since the reactive pulse is much higher, it makes sense that the average unsteady CD would be lower for a similar pressure ratio.

## V. Conclusion

In summary, this method of unsteady simulation of RDC injectors provides insight into how these injectors react to the shockwave that travels around an RDC. A two-dimensional injector with a cyclic pressure wave coming from an RDE simulation is taken as a forcing function. Several parameters are used to determine injector behavior such as the total mass injected over 1 cycle, average hot flow discharge coefficient and the unsteady discharge coefficient. The difference between a steady simulation and unsteady simulation in terms of discharge coefficient is documented with discharge coefficients up to 0.9 for steady flows and dropping to 0.4 during hot flow operation. Additionally, the unsteady discharge coefficient as a function of cycle time is plotted to demonstrate the steady discharge is never achieved. The baseline injector does not reach the steady C<sub>d</sub> during these simulations. The 2D unwrapped simulations bridge the gap between low fidelity simulations and system performance by simplifying the full RDC into a 2D plane. The results are performance for the whole RDC that could be explored in experimental testing. Single injector validation was completed experimentally and compared with CFD of the same geometries. The resulting figure showed the correlation in full experimental testing and the reduced computational methods defined. Future work would include expanding to full RDC simulations to compare with 2D unwrapped as well as experimental testing with a full RDC of new injector geometries. Similar methods could also be used to preliminarily simulate other important aspects of an RDC such as cooling and thrust predictions.

# Acknowledgements

This work is funded by a NASA Phase 2 SBIR.

#### References

- [1] Paxson, Daniel E. "Numerical analysis of a rotating detonation engine in the relative reference frame." 52nd Aerospace Sciences Meeting. 2014.
- [2] Athmanathan, V., Braun, J., Ayers, Z.M., Fugger, C.A., Webb, A.M., Slipchenko, M.N., Paniagua, G., Roy, S. and Meyer, T.R., 2022. On the effects of reactant stratification and wall curvature in non-premixed rotating detonation combustors. Combustion and Flame, 240, p.112013.
- [3] Teasley, T. W., Protz, C. S., Larkey, A. P., Williams, B. B., and Gradl, P. R., "A review towards the design optimization of high performance additively manufactured rotating detonation rocket engine injectors," AIAA Propulsion and Energy 2021 Forum, Jul. 2021.
- [4] Duvall, James, et al. "Study of the effects of various injection geometries on the operation of a rotating detonation engine." 208 AIAA Aerospace sciences meeting. 2018.
- [5] Keller, A. R., Otomize, J., Nair, A. P., Minesi, N. Q., and Spearrin, R. M., "High-Diodicity Impinging Injector Design for Rocket Propulsion Enabled by Additive Manufacturing," 2022. https://doi.org/10.2514/6.2022-1265
- [6] Bigler, Blaine R., et al. "Injector alignment study for variable mixing in rotating detonation rocket engines." AIAA Scitech 2019 Forum. 2019.
- [7] Pryor, Jeremy & Weightman, Joel & Sandberg, Richard & Bohon, Myles & Edgington-Mitchell, Daniel. (2024). Shock Propagation Through a Square Injector: Investigation into Rotating-Detonation Engine Injector Dynamics. AIAA Journal. 1-15. 10.2514/1.J064217.
- [8] Zhao, Majie, and Huangwei Zhang. "Large eddy simulation of non-reacting flow and mixing fields in a rotating detonation engine." Fuel 280 (2020): 118534.
- [9] Gaillard, Thomas, Dmitry Davidenko, and Francis Dupoirieux. "Numerical investigation of an unsteady injection adapted to the continuous detonation wave rocket engine operation." Progress in propulsion physics 11 (2019): 347-370.
- [10] Chakravarthy S, Peroomian O, Goldberg U, Palaniswamy S. The CFD ++ computational fluid dynamics software suite. AIAA and SAE. World Aviation Conference Anaheim, CA; 1998. doi: 10.2514/6.1998-5564
- [11] J. Grunenwald "INVESTIGATION OF ROTATING DETONATION PHYSICS AND DESIGN OF A MIXER FOR A ROTATING DETONATION ENGINE", 2023
- [12] Casiano, M. J., Hulka, J. R., and Yang, V., "Liquid-propellant rocket engine throttling: A comprehensive review," *Journal of Propulsion and Power*, vol. 26, Sep. 2010, pp. 897–923.
- [13] V, Athmanathan, J. Braun, Z. M. Ayers, C. A. Fugger, A. M. Webb, M. N. Slipchenko, G. Paniagua, S. Roy, T. R. Meyer, On the effects of reactant stratification and wall curvature in non-premixed rotating detonation combustors [14] S. Yao, X. Tang, M. Luan, J. P. Wang Numerical study of hollow rotating detonation engine with different fuel injection area ratios, Proc. Combust. Inst. 34 (2017) 2649-2655
- [15] Waxman, B. S., "AN INVESTIGATION OF INJECTORS FOR USE WITH HIGH VAPOR PRESSURE PROPELLANTS WITH APPLICATIONS TO HYBRID ROCKETS," dissertation, 2014.
- [16] Lim, D., Heister, S., Stechmann, D. *et al.* Transient response of a liquid injector to a steep-fronted transverse pressure wave. *Shock Waves* **28**, 919–932 (2018). https://doi.org/10.1007/s00193-017-0787-8
- [17] Teasley, T., Williams, B., Larkey, A., Protz, C., and Gradl, P., "A Review Towards the Design Optimization of High-Performance Additively Manufactured Rotating Detonation Rocket Engine Injectors," 2021. https://doi.org/10.2514/6.2021-3655
- [18] Hoeper, M. W., Webb, A. M., Athmanathan, V., Wang, R. B., Douglas Perkins, H., Roy, S., Meyer, T. R., and Fugger, C. A., "Liquid Fuel Refill Dynamics in a Rotating Detonation Combustor Using Megahertz Planar Laser-Induced Fluorescence," Proceedings of the Combustion Institute, Vol. 39, No. 3, 2023, pp. 3051–3061. https://doi.org/10.1016/j.proci.2022.07.230
- [19] Athmanathan, V., Fisher, J. M., Ayers, Z., Cuadrado, D. G., Andreoli, V., Braun, J., Meyer, T., Paniagua, G., Fugger, C. A., and Roy, S., "Turbine-Integrated High-Pressure Optical RDE (THOR) for Injection and Detonation Dynamics Assessment," 2019. https://doi.org/10.2514/6.2019-4041
- [20] Athmanathan, V., Braun, J., Ayers, Z. M., Fugger, C. A., Webb, A. M., Slipchenko, M. N., Paniagua, G., Roy, S., and Meyer, T. R., "On the Effects of Reactant Stratification and Wall Curvature in Non-Premixed Rotating Detonation Combustors," Combustion and Flame, Vol. 240, 2022. <a href="https://doi.org/10.1016/j.combustflame.2022.112013">https://doi.org/10.1016/j.combustflame.2022.112013</a>